RSC Advances

This is an *Accepted Manuscript*, which has been through the Royal Society of Chemistry peer review process and has been accepted for publication.

Accepted Manuscripts are published online shortly after acceptance, before technical editing, formatting and proof reading. Using this free service, authors can make their results available to the community, in citable form, before we publish the edited article. This *Accepted Manuscript* will be replaced by the edited, formatted and paginated article as soon as this is available.

You can find more information about *Accepted Manuscripts* in the Information for Authors.

Please note that technical editing may introduce minor changes to the text and/or graphics, which may alter content. The journal's standard Terms & Conditions and the Ethical guidelines still apply. In no event shall the Royal Society of Chemistry be held responsible for any errors or omissions in this *Accepted Manuscript* or any consequences arising from the use of any information it contains.

ROYAL SOCIETY OF CHEMISTRY

www.rsc.org/advances

One-Step Synthesis of Trimetallic Pt-Pd-Ru Nanodendrites as Highly Active Electrocatalysts

Kamel Eid,[a,b] Victor Malgras,[c] Pei He,[d] Kunmiao Wang,[d] Ali Aldalbahi,[e]

Saad M. Alshehri,[e] Yusuke Yamauchi,[c] and Liang Wang [a,*]

[a] State Key Laboratory of Electroanalytical Chemistry, Changchun Institute of Applied Chemistry, Chinese Academy of Sciences, Changchun, Jilin 130022, P.R. China

[b] University of Chinese Academy of Sciences, Beijing 100039, P.R. China

[c] World Premier International (WPI) Research Center for Materials Nanoarchitectonics (MANA), National Institute for Materials Science (NIMS), 1-1 Namiki, Tsukuba, Ibaraki 305-0044, Japan

[d] Key Laboratory of Tobacco Chemistry of Yunnan Province, China Tobacco Yunnan Industrial Co. Ltd, Kunming, Yunnan 650231, P.R. China

[e] Department of Chemistry, College of Science, King Saud University, Riyadh 11451, Saudi Arabia

*Corresponding Author's E-mail: wangliang@ciac.ac.cn

RSC Advances Accepted Manuscript

Abstract

The precise control over the composition and the structure is highly important for designing highly active nanostructured electrocatalysts. Herein, we report a one-step strategy to directly synthesize trimetallic Pt-Pd-Ru nanodendrites in an aqueous solution at room temperature. These newly designed nanodendrites exhibit superior catalytic activities for both methanol oxidation reaction (MOR) and oxygen reduction reaction (ORR) in comparison with bimetallic Pt-Pd nanoflowers and commercially available Pt/C catalysts.

RSC Advances Accepted Manuscript

1. Introduction

Platinum (Pt) is an effective catalyst for various reactions such as methanol oxidation reaction (MOR) and oxygen reduction reaction (ORR).[1-5] However, its stability, its readiness to be contaminated by carbon monoxide and its high cost are critical issues that need to be addressed. Considerable efforts have been devoted to overcome these problems, predominantly focusing on controlling the morphology, size and composition of Pt-based nanocrystals (NCs).[4-8] For instance, Pt nanorods with a high density of mesopores have exhibited enhanced performance in MOR, compared to Pt nanorods and mesoporous Pt nanoparticles,[9] and concaved Pt nanocubes have showed higher electrocatalytic performance for ORR in comparison with normal Pt cubes.[10] Recent progress has demonstrated that bimetallic Pt-based NCs show improved catalytic activities benchmarked against monometallic Pt NCs. For example, concaved Pt-Pd nanoparticles show higher activity for MOR than dendritic Pt nanoparticles,[11] and mesoporous PtRu alloy exhibits enhanced performance for MOR in relative to mesoporous Pt.[12] Thus, synthesis of Pt-based NCs has attracted considerable interest to date. Rational design of composition and structure is critical to design highly active Pt catalysts.[1, 4, 7, 13]

Trimetallic NCs with designed composition and morphology can provide new insights on the catalytic properties of Pt-based materials which have been rarely reported in comparison with Pt-based mono- and bi-metallic catalysts. Several approaches, such as seed-mediated growth, thermal decomposition, and galvanic replacement, have been explored for the synthesis of Pt-based trimetallic NCs in pioneering studies.[14-19] For example, Au@CuPt NCs which are highly active catalysts for both MOR and ORR are synthesized by a seed-mediated growth combined with thermal decomposition,[2] FePtCu nanorods which are active ORR catalysts are prepared by thermal decomposition,[16] active Au@PdPt NCs for MOR are synthesized with dual reducing agents,[19] and efficient PtPdTe nanowires for MOR are prepared by using Te nanowires as both sacrificial template and reducing agent.[20] Until now, there have been only few reports on Pt-based trimetallic NCs, which have been rarely achieved through facile synthetic methods.[21] The development of a simple and effective route for scalable synthesis of Pt-based trimetallic NCs with desired compositions and structures leading to specific catalytic activities is a quite challenging issue.

Our target in this study is to develop a one-step and effective approach for the synthesis of trimetallic

RSC Advances Accepted Manuscript

Pt-Pd-Ru nanodendrites in an aqueous reaction solution at room temperature without the need for any seed, template, organic solvent and heating treatment. The newly designed Pt-Pd-Ru nanodendrites exhibit superior electrocatalytic performance for both MOR and ORR in comparison with bimetallic Pt-Pd nanoflowers and commercial available Pt/C catalysts.

2. Experimental section

Materials. $RuCl_3$, K_2PtCl_4, Na_2PdCl_4, L-ascorbic acid (AA), $NaBH_4$, HCOOH and methanol were obtained from Beijing Chemical Reagent (Beijing, China). Pluronic F127 was purchased from Sigma-Aldrich Co. Commercial Pt/C catalyst was ordered from Alfa Aesar Co.

Synthesis of trimetallic Pt-Pd-Ru nanodendrites. Trimetallic nanodendrites were synthesized by mixing 0.9 mL of 20 mM $RuCl_3$(aq), 0.9 mL of 20 mM Na_2PdCl_4(aq), 1.2 mL of 20 mM K_2PtCl_4(aq) and 0.01g Pluronic F127. Then, 0.3 mL of 0.4 M AA solution was quickly added under stirring. The reaction solution was kept under stirring for 3 h at room temperature. The product was collected by consecutive washing/centrifugation cycles for three times with water. The collected product was dispersed in water by sonicating for further characterizations.

Synthesis of bimetallic Pt-Pd nanoflowers. According to our previous report,[6] Pt-Pd nanoflowers were prepared by mixing 0.3 mL of 5 mM Na_2PdCl_4(aq), 0.7 mL of 15 mM K_2PtCl_4(aq), and 0.01g Pluronic F127. Then, 1 mL of 0.4 M AA solution was added. The reaction solution was kept under stirring for 3 h at room temperature. The final product was collected as mentioned previously.

Characterizations. The particle size and morphology were investigated by a Hitachi H-8100 transmission electron microscope (TEM) with an accelerating voltage of 100 kV and a JEM-2010 with an accelerating voltage of 200 kV. X-ray diffraction pattern was recorded on a D8 ADVANCE (Bruker AXS, Germany) diffractometer using Cu Kα radiation. X-ray photoelectron spectroscopy (XPS) analysis was carried out on an ESCALAB MK II spectrometer (VG Scientific, UK) with Al Kα X-ray radiation for excitation.

Electrochemical analysis. Cyclic voltammograms (CVs), linear sweep voltammograms (LSVs), and chronoamperometric experiments were performed using a CHI 832C electrochemical analyzer (Chenhua Co., Shanghai, China). A conventional three-electrode cell was used, including a Ag/AgCl (saturated KCl) electrode as the reference electrode, a Pt wire as the counter electrode and the working electrode. The

RSC Advances Accepted Manuscript

working electrode was a modified glassy carbon electrode (GCE) (3 mm in diameter) coated with 10 μg of the different catalysts and dried at room temperature. Then, 3 μL of Nafion (0.05 %) was coated on the surface of the modified GCE and dried before electrochemical experiments.

MOR measurements were carried out in a 0.1 M N_2-saturated $HClO_4$ solution containing 1 M methanol at a scan rate of 50 mV s^{-1}. MOR durability tests were performed at 0.6 V with a scan rate of 50 mV s^{-1} for 2000 cycles. ORR measurements were performed on a RRDE-3A rotation system (ALS Co. Ltd, Japan) with a rotating disk electrode (RDE) in a 0.1 M O_2-staurtaed $HClO_4$ solution with a rotation speed of 1,600 rpm at a scan rate of 10 mV s^{-1}. ORR durability tests were conducted between 0 and 1 V with a rotation speed of 1,600 rpm at a scan rate of 10 mV s^{-1} for 5000 cycles.

The electrochemically active surface area (ECSA) can be calculated by the following equation:

$$\text{ECSA} = Q_H/m \times 210$$

where, Q_H is the charge for H_{upd} adsorption determined using $Q_H = 0.5 \times Q$, where Q is the is the charge in the H_{upd} adsorption /desorption area obtained after the double layer correction region, between 0 and 0.37 V, m is the Pt loading amount on the electrode, and 210 μC cm^{-2} is the charge required for monolayer adsorption of hydrogen on Pt surface.

The Koutecky-Levich equation was used to calculate the kinetic current, which can be described as follow:

$$\frac{1}{j} = \frac{1}{j_k} + \frac{1}{j_d}$$

Where j, j_k and j_d are the measured, kinetic and diffusion-limited current densities, respectively. Then, the kinetic current was calculated based on the following equation:

$$j_k = \frac{j \times j_d}{j_d - j}$$

3. Results and discussion

Fig. 1a-b shows TEM images of as-prepared trimetallic Pt-Pd-Ru nanodendrites synthesized by one-step reduction of the metallic precursors with AA in an aqueous solution containing Pluronic F127 at room temperature. Well-dispersed nanoparticles with uniform dendritic shape are observed without any

RSC Advances Accepted Manuscript

byproducts. The nanoparticles size ranges from 16 to 43 nm and the average diameter is ~ 22 nm. The energy-dispersive X-ray (EDX) spectrum reveals that the elemental compositions of the nanoparticles include Ru, Pd and Pt, the atomic ratio of Ru/Pd/Pt is 1/2.5/5.5, which is confirmed EDX analysis **(Fig. 1 c)**.Both elemental mappings and cross-sectional compositional line profiles clearly confirm that the three elements (Pt, Pd, and Ru) are uniformly distributed throughout the nanoparticle (**Fig. 1d**). Pt is slightly concentrated at the surface of the particle. **Fig. 2a** shows a highly magnified TEM image of one nanoparticle. The nanoparticle has a permeable dendritic exterior with branches having a diameter ranging from 2 to 4 nm. The *d*-spacing is 0.23 nm and can be assigned to the (111) plane of a face-centered cubic (*fcc*) structure (**Fig. 2b-c)**.

The wide-angle XRD pattern of the as-made nanoparticles shows several intense peaks which can be assigned to the (111), (200) and (220) diffraction planes of a *fcc* crystal (**Fig. S1**). Thus, the obtained nanoparticles are predominately crystalized into a *fcc* structure. Due to a very high lattice match between Pt and Pd (99.23%), the peaks of the two elements in the XRD pattern are overlapped. It is important to mention that each peak is slightly shifted, indicating that the Ru atoms with smaller size have been successfully incorporated into the Pt/Pd *fcc* crystalline structure. Other additional peaks are assigned to a typical *hcp* Ru structure. Thus, a certain amount of Ru content separately exists without alloying with other Pt and Pd metals. XPS is employed to gain insight on the chemical state of the three metals (**Fig. S2**). The presence of peaks of Pt 4*f* (71.05 eV and 74.50 eV), Pd 3*d* (335.3 eV) and Ru 3*p* (463.2 and 486.2 eV) confirms that collateral oxides are inexistent or negligible.

In order to explore the formation process of the trimetallic nanodendrites, three sequential products sampled at different reaction times are imaged by TEM. As shown in **Fig. S3**, spherical nanoparticles are initially formed, acting as in-situ seeds for the sequent deposition. Pluronic F127 plays a structure-directing role to direct the dendritic metal deposition.[6] The use of AA as a soft reducing agent is one of the critical factor for the formation of the trimetallic nanodendrites. The use of reducing agents with different reductive capabilities can lead to different reduction rates for different metallic precursors during the synthesis.[21, 24] The attempt of replacing of AA with formic acid, a weak reducing agent, under the typical synthetic condition can also successfully produce nanodendrites, while the use of sodium borohydride, a strong

RSC Advances Accepted Manuscript

reducing agent, is unsuccessful, resulting in irregular nanostructures (**Fig. S4**). The reduction rate determines nucleation kinetic which strongly affects the formation of the nanoparticles.[4, 13, 21, 24-26] A mild reducing agent, such as AA or formic acid, allows favorable homogeneous nucleation of initial in-situ seeds, providing sufficient nucleation sites and reaction times for subsequent metallic depositions, while a strong reducing agent, such as sodium borohydride, immediately reduces the whole metallic precursor which leads to a poor isolation of nucleation sites and an uncontrollable growth process.[21, 25, 26]

Moreover, the concentration of reducing agent is also important. Quasi-spherical nanoparticles are produced with 0.1 M AA while further increase of the AA concentration up to 0.2 M leads to the formation of nanoparticles with dendritic shape (**Fig. S5**). Using a AA concentration of 0.4 M is favorable for high quality synthesis (**Fig. 1a**). The use of nonionic surfactant Pluronic F127 as a capping agent is another key factor to synthesize the trimetallic nanodendrites. If a cationic surfactant such as cetyltrimethylammonium chloride (CTAC) is used as capping agent instead, irregular nanostructures are obtained (**Fig. S6**). Cationic surfactant easily bonds with the metallic precursors through electrostatic interactions and tends to precipitate, which is unfavorable to control the synthesis. Furthermore, the concentration of Pluronic F127 is also important. When the synthesis was achieved without Pluronic F127 or with a 10-times lower concentration (0.001 g), spherical nanoparticles without branches are produced and the nanoparticles tend to aggregate (**Fig. S7**). Using a concentration of 0.01 g favors formation of dendritic nanoparticles (**Fig. 1a**). The length of the Pt branches can be effectively controlled by simply adjusting the amount of Pt precursor in the initial solution. A higher Pt precursor amount favors the growth of the branches because of the sufficient Pt atomic addition and (**Fig. 1a and Fig. S8**).[6]

Bimetallic nanodendrites, especially core-shell structured metallic nanoparticles, are usually prepared by a seed-mediated growth strategy in which two-step synthesis are necessary.[4] For instance, Au@Pt nanodendrites are successfully formed by using Au nanoparticles as seeds for the subsequent Pt branch growth at 100 °C.[26] For the preparation of multilayered core-shell nanoparticles, multiple step synthesis is necessary. For example, nanocrystals composed of Pd and Pt alternated layers are obtained by multiple step synthesis at 90 °C.[27] In most cases, the obtained nanoparticles show a significant lack of nanoporosity. For instance, Au@Pd core-shell nanooctahedrons with smooth exteriors are prepared by co-reducing Au and Pd

RSC Advances Accepted Manuscript

precursors in the presence of CTAC at 90 °C for 48 h.[28] The present synthetic approach is favorable for the synthesis of trimetallic NCs with desired shape by a very simple route at room temperature in an aqueous solution (**Table S1**). The proposed synthetic approach reported here shows obvious advantages over the traditional approaches that involve multiple steps and high temperatures.

As-prepared trimetallic Pt-Pd-Ru nanodendrites are considered as a promising catalyst for MOR and their electrocatalytic performance has been further benchmarked against bimetallic Pt-Pd nanoflowers and commercially available commercial Pt/C catalysts. **Fig. 3a** shows the CVs of the three catalysts recorded at room temperature in a N_2-saturated 0.1 M $HClO_4$ solution at a sweep rate of 50 mV s^{-1}. The electrochemical surface area (ECSA) of trimetallic Pt-Pd-Ru nanodendrites (65.1 $m^2 g^{-1}$) is higher than those of bimetallic Pt-Pd nanoflowers (32 $m^2 g^{-1}$) and Pt/C (45.2 $m^2 g^{-1}$). **Fig. 3b** displays the CVs of the catalysts measured in a 0.1 M $HClO_4$ aqueous solution with 1 M CH_3OH at a sweep rate of 50 mV s^{-1}, which are normalized in reference to the geometric area of working electrode. The current density of Pt-Pd-Ru nanodendrites in the positive scan (6.2 mA cm^{-2}) is 2.9 times higher than Pt-Pd nanoflowers (2.1 mA cm^{-2}) and 11.3 times higher than Pt/C (0.55 mA cm^{-2}), respectively. **Fig. 3c** further shows the comparisons of the specific activities (current densities are normalized by ECSA) and mass activities (current densities are normalized by Pt mass) of the three materials. The activity of Pt-Pd-Ru nanodendrites is higher than those of Pd-Pt nanodendrites and Pt/C in terms of both specific activity and mass activity. The specific activity of Pt-Pd-Ru nanodendrites (3.0 mA cm^{-2}) is 2.5 times higher than that of Pt-Pd nanoflowers (1.2 mA cm^{-2}) and 8.6 times higher than that of Pt/C (0.35 mA cm^{-2}), respectively. The mass activity of Pt-Pd-Ru nanodendrites (1.82 mA μg^{-1}) is 3.0 and 11.4 times higher than those of Pt-Pd nanoflowers (0.61 mA μg^{-1}) and Pt/C (0.16 mA μg^{-1}), respectively, and is higher than those of Pt-Ru nanoparticles (0.21 mA μg^{-1}) and Pd-Ru nanoparticles (0.02 mA μg^{-1}).The durability tests further reveal that Pt-Pd-Ru nanodendrites display a much higher current stability after 2,000 cycles compared to the referenced catalysts (**Fig. 3d)**. Such a high durability of Pt-Pd-Ru nanodendrites is attributed to the stability of the initial ECSA. After 2000 cycles, the Pt-Pd-Ru nanodendrites retain 88 % of its initial ECSA (57.2 $m^2 g^{-1}$). In a comparison, Pt/C preserves 54 % of its initial ECSA (24.3 $m^2 g^{-1}$) (**Fig. S9**).

To get more insight on their catalytic properties, the ORR activity of the Pt-Pd-Ru nanodendrites is

RSC Advances Accepted Manuscript

further investigated in comparison with Pt-Pd nanoflowers and Pt/C catalysts in an O_2 saturated 0.1 M $HClO_4$ solution with a rotation speed of 1600 rpm at a scan rate of 10 mV s^{-1}. The ORR polarization curves, which are normalized in reference to the geometric area of working electrode, reveal that the half-wave potential of Pt-Pd-Ru nanodendrites (0.55 V) is more positive than those of Pt-Pd nanoflowers (0.48 V) and Pt/C (0.45 V) (**Fig. 4a**). From Koutecky-Levich plots, the electron transfer numbers (*n*) for Pt-Pd-Ru nanodendrites and Pt-Pd nanoflowers are 3.88 and 3.76, respectively. The mass activity of Pt-Pd-Ru nanodendrites (1.5 mA μg^{-1}) is 3 times higher than that of Pt-Pd nanoflowers (0.5 mA μg^{-1}) and 8.5 times higher than that of Pt/C (0.18 mA μg^{-1}), meanwhile, the specific activity of Pt-Pd-Ru nanodendrites (1.95 mA cm^{-2}) is 1.8 and 4.8 times higher than those of Pt-Pd nanoflowers (1.09 mA cm^{-2}) and Pt/C (0.4 mA cm^{-2}), respectively (**Fig. 4b**). The mass activity of Pt-Pd-Ru nanodendrites (1.5 mA μg^{-1}) is higher than that of Pt-Ru nanoparticles (0.17 mA μg^{-1}), and Pd-Ru nanoparticles is inactive. The results clearly show that the Pt-Pd-Ru nanodendrites exhibit very high electrocatalytic activity in terms of both mass activity and specific activity. It is noted that the mass activity of our Pt-Pd-Ru nanodendrites for ORR is also superior to previously reported PtFeCu nanorods, PtPdBi nanowires, PtNiFe nanocubes, PtCuCo nanospheres (**Table S2)**. Moreover, our Pt-Pd-Ru nanodendrites and Pt/C exhibit 2 and 20 mV degradation in the half-wave potential, respectively, after 5000 cycles, which clearly demonstrates that our Pt-Pd-Ru nanodendrites exhibit superior durability for ORR in comparison with Pt/C (**Fig. 4c-d**). The enhanced performance of the Pt-Pd-Ru nanodendrites is considered to be attributed to its morphology and composition. Its dendritic structure not only provides sufficient accessible active sites but also favors the tolerance to undesirable active site agglomeration. Alloying Pt with Pd and Ru alters the electronic structures of Pt and enhances the electron mobility and subsequent electrocatalytic kinetic.[5,10,19,27], which subsequently reduces the binding energies for oxygen species onto Pt-Pd-Ru nanodendrites and improves the poison tolerance. Based on the above electrochemical investigations, it can be concluded that the Pt-Pd-Ru nanodendrites are suited for highly active electrocatalysts with superior durability for both MOR and ORR.

Conclusion

A direct and efficient strategy for one-step synthesis of trimetallic Pt-Pd-Ru nanodendrites in an aqueous solution at room temperature is presented. The obtained trimetallic Pt-Pd-Ru nanodendrites exhibit

RSC Advances Accepted Manuscript

superior catalytic performance for both MOR and ORR in comparison with bimetallic Pt-Pd nanoflowers and Pt/C, and can be considered as promising electrocatalysts for future electrochemical energy conversion.

Acknowledgements

This work was supported by the National Natural Science Foundation of China (No. 21273218). Kamel Eid greatly appreciates the TWAS-UCAS President Fellowship. Ali Aldalbahi acknowledges the financial support by Deanship of Scientific Research, College of Science Research Center, King Saud University.

RSC Advances Accepted Manuscript

References

1. D. Wang, H. Xin, R. Hovden, H. Wang, Y. Yu, D. Muller, F. DiSalvo and H. Abruña, *Nat. Mater.*, 2013, **12**, 81-87.
2. X. Sun, D. Li, Y. Ding, W. Zhu, S. Guo, Z. Wang and S. Sun, *J. Am. Chem. Soc.*, 2014, **136**, 5745-5749.
3. C. Chen, Y. Kang, Z. Huo, Z. Zhu, W. Huang, H. Xin, J. Snyder, D. Li, J. Herron, M. Mavrikakis, M. Chi, K. More, Y. Li, N. Markovic, G. Somorjai, P. Yang and V. Stamenkovic, *Science*, 2014, **343**, 1339-1343.
4. J. Wu and H. Yang *Acc. Chem. Res.*, 2013, **46**, 1848-1857
5. S. Pethaiah, M. Ulaganathan, M. Viswanathan and S. Chan, *RSC Adv.,* 2015, **5**, 981-987.
6. L. Wang and Y. Yamauchi, *Chem. Asian J.*, 2010, **5**, 2493-2498.
7. C. Cui, L. Gan, M. Heggen, S. Rudi, and P. Strasser, *Nat. Mater.*, 2013, **12**, 765-771.
8. M. Gong, G. Fu, Y. Chen, Y. Tang, and T. Lu, *ACS Appl. Mater. Interfaces*, 2014, **6**, 7301-7308.
9. C. Li, T. Sato and Y. Yamauchi, *Angew. Chem. Int. Ed.*, 2013, **52**, 8050-8053.
10. T. Yu, D. Kim, H. Zhang and Y. Xia, *Angew. Chem., Int. Ed.*, 2011, **50**, 2773-2777.
11. H. Ataee-Esfahani, M. Imura, and Y. Yamauchi, *Angew. Chem. Int. Ed.*, 2013, **52**, 13611-13615.
12. H. Wang, M. Imura, Y. Nemoto, L. Wang, H. Jeong, T. Yokoshima, O. Terasaki and Y. Yamauchi, *Chem. Eur. J.*, 2012, **18**, 13142-13148.
13. Y. Xu and B. Zhang, *Chem. Soc. Rev.*, 2014, **43**, 2439-2450.
14. S. Zhang, S. Guo, H. Zhu, D. Su and S. Sun, *J. Am. Chem. Soc.*, 2012, **134**, 5060-5063.
15. S. Guo, S. Zhang, X. Sun and S. Sun, *J. Am. Chem. Soc.*, 2011, **133**, 15354-15357.
16. H. Zhu, S. Zhang, S. Guo, D. Su and S. Sun, *J. Am. Chem. Soc.*, 2013, **135**, 7130-7133.
17. S. Chou, J. Shyue, C. Chien, C. Chen, Y. Chen and P. Chou, *Chem. Mater.*, 2012, **24**, 2527-2533.
18. H. Liao and Y. Hou, *Chem. Mater.*, 2013, **25**, 457-465.
19. a) S. Kang, Y. Lee, Y. Park, B. Choi, J. Hong, K. Park and S. Han, *ACS Nano*, 2013, **7**, 7945-7955; b) S. Choi, M. Shao, N. Lu, A. Ruditskiy, H-C Peng, J. Park, S. Guerrero, J. Wang, M. J. Kim and Y.

RSC Advances Accepted Manuscript

Xia, *ACS Nano*, 2014, **8**, 10363-10371; c) B. Singh, L. Murad, F. Laffir, C. Dickinsonb and E. Dempsey, *Nanoscale*, 2011, **3**, 3334-3349; d) S. Fosdick, S. Berglund, C .Mullins and R. Crooks, ACS Catalysis, 2014. **4**, 1332-1339; e) D. Huang, P. He, Q. Yuan and X. Wang, *Chem. Asian J.*, 2015, **10**, 608-613; f) T. Huan, D. Shinde, S. Kim, S. Han, V. Artero and H. Chung, *RSC Adv.*, 2015, **5**, 6940-6944; g) X. Liu, G. Fu, Y. Chen, Y. Tang, P. She and T. Lu, Chem. *European J.*, 2014, **20**, 585-590; h) W. Wang, R. Wang, H. Wang, S. Ji, J. Key, X. Li, and Z. Lei, *J. Power Sources,* 2011, **196**, 9346-9351.

20. H. Li, S. Zhao, M. Gong, C. Cui, D. He, H. Liang, L. Wu and S. Yu, *Angew. Chem. Int. Ed.*, 2013, **52**, 7472-7476.
21. L. Wang and Y. Yamauchi, *J. Am. Chem. Soc.*, 2010, **132**, 13636-13638.
22. H. Ataee-Esfahani, Y. Nemoto, M. Imura, and Y. Yamauchi, *Chem. Asian J.*, 2012, **7**, 876-880.
23. Q. He, B. Shyam, M. Nishijima, X. Yang, B. Koel, F. Ernst, D. Ramaker, and S. Mukerjee, *J. Phys. Chem. C*, 2013, **117**, 1457-1467.
24. W. Yu, M. Porosoff and J. Chen, *Chem. Rev.,* 2012, **112**, 5780-5817.
25. H. Zhang, M. Jin and Y. Xia, *Chem. Soc. Rev.*, 2012, **41**, 8035-8049.
26. Y. Kim, J. Hong, Y. Lee, M. Kim, D. Kim, W. Yun and S. Han, *Angew. Chem. Int. Ed.*, 2010, **49**, 10197-10201.
27. H. Zhang, M. Jin, J. Wang, M. Kim, D. Yang and Y. Xia, *J. Am. Chem. Soc.*, 2011, **133** 10422-10425.
28. Y. Lee, M. Kim, Z. Kim and S. Han, *J. Am. Chem. Soc.*, 2009, **131**, 17036-17037.

RSC Advances Accepted Manuscript

Figures and Figure Captions

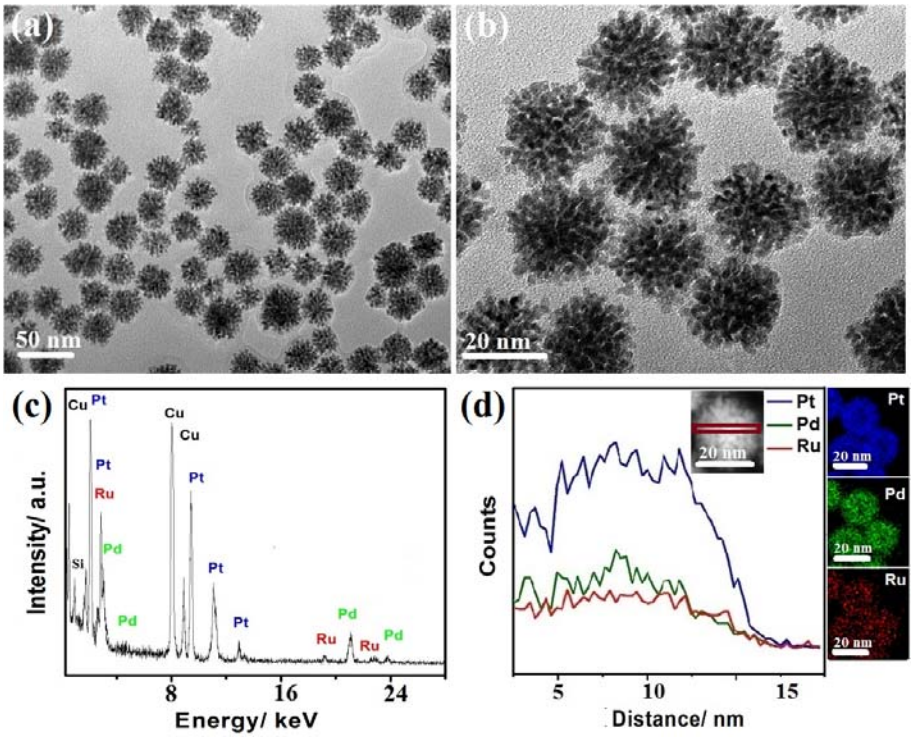

Fig. 1 (a and b) TEM images at different magnifications, (c) EDX spectrum and (d) EDX elemental mapping of the trimetallic Pt-Pd-Ru nanodendrites.

RSC Advances Accepted Manuscript

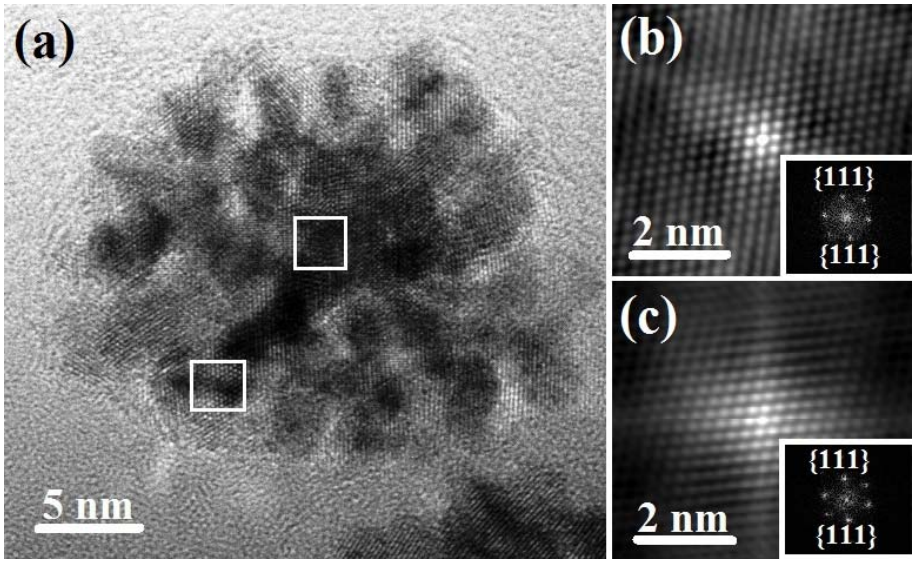

Fig. 2 (a) Highly magnified TEM image of one trimetallic Pt-Pd-Ru nanodendrite. The lattice fringes in the shell area (b) and in the core area (c). The inserts in b and c display the corresponding FFT patterns.

RSC Advances Accepted Manuscript

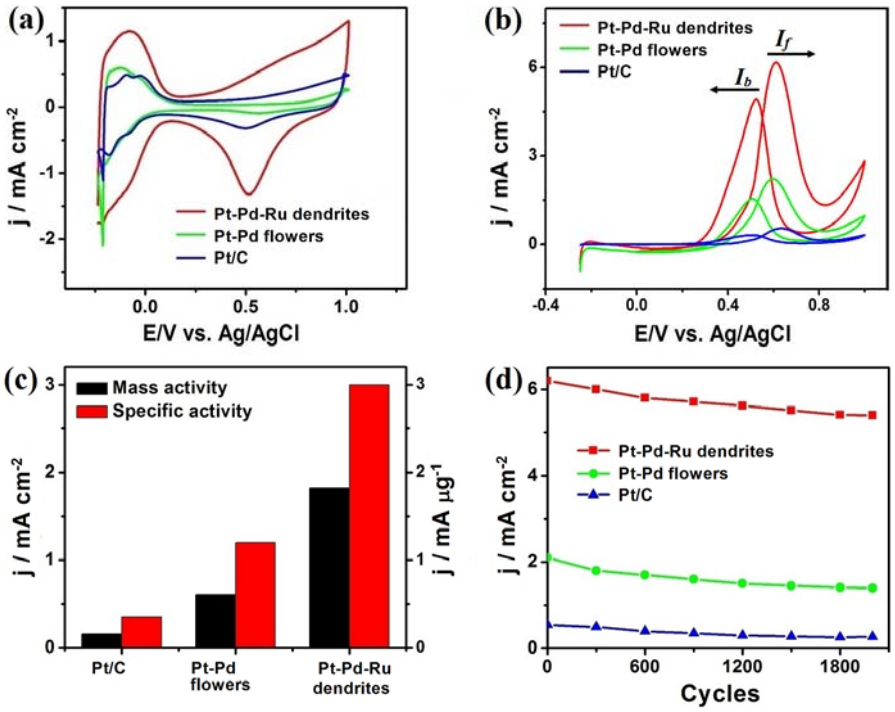

Fig. 3 CVs of trimetallic Pt-Pd-Ru nanodendrites, bimetallic Pt-Pd nanoflowers and Pt/C in 0.1 M $HClO_4$ in the absence (a) and presence of 1 M CH_3OH (b) at a scan rate of 50 mV s^{-1}. (c) The comparisons of the mass activities and specific activities of the three materials at 0.6 V. (d) Durability for 2000 cycles in 0.1 M $HClO_4$ presence of 1 M CH_3OH at 0.6 V. In (a), (b) and (d), current densities are normalized in reference to the geometric area of the working electrode. In (c), specific and mass activities are normalized in reference to the ECSAs and loading amount of Pt, respectively. In (b), I_f and I_b are the forward and backward current densities, respectively.

RSC Advances Accepted Manuscript

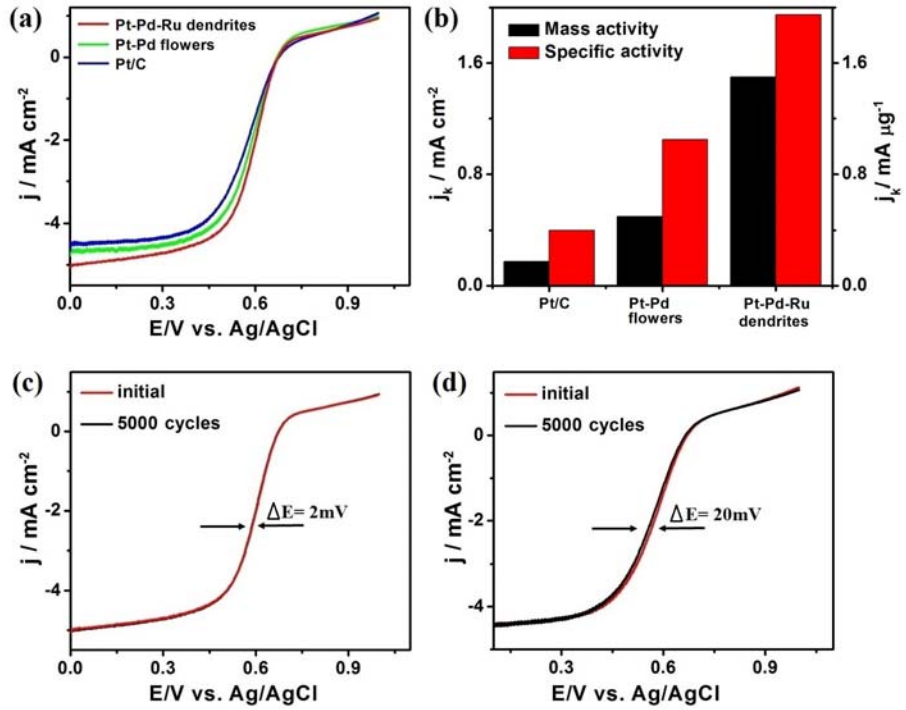

Fig. 4 (a) ORR polarization curves and (b) the comparisons of mass activities and specific activities of trimetallic Pt-Pd-Ru nanodendrites, bimetallic Pt-Pd nanoflowers, and Pt/C at 0.6 V. The ORR polarization curves before and after durability test for trimetallic Pt-Pd-Ru nanodendrites, bimetallic Pt-Pd nanoflowers, (c) and Pt/C (d). All the polarization curves are measured in an O_2 saturated 0.1 M $HClO_4$ solution at a scan rate of 10 mV s^{-1} with a rotation speed of 1600 rpm. In (a), (c) and (d), current densities are normalized in reference to the geometric area of the working electrode. In (b), specific and mass activities are normalized in reference to the ECSAs and loading amount of Pt, respectively.

RSC Advances Accepted Manuscript

Graphical Abstract

Trimetallic Pt-Pd-Ru nanodendrites synthesized by a one-step route are highly active electrocatalysts for methanol oxidation reaction and oxygen reduction reaction.

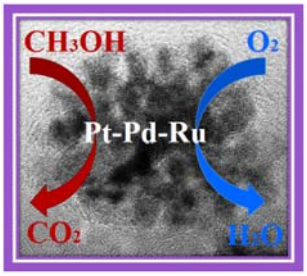

RSC Advances Accepted Manuscript